Journal of Fluorescence
https://doi.org/10.1007/s10895-019-02405-0

ORIGINAL ARTICLE

Identifying the Stoichiometry of Metal/Ligand Complex by Coupling Spectroscopy and Modelling: a Comprehensive Study on Two Fluorescent Molecules Specific to Lead

William René [1,2,3] **· Madjid Arab** [2] **· Katri Laatikainen** [4] **· Stéphane Mounier** [3] **· Catherine Branger** [1] **· Véronique Lenoble** [3]

Received: 10 May 2019 / Accepted: 24 June 2019

Abstract

Two new chemosensors for lead (II) were synthesized based on 5-((anthracen-9-ylmethylene) amino)quinolin-10-ol (ANQ). ANQ was modified in the para position of the imine group via a methoxy link either with methylmethacrylate (ANQ-MMA) or styrene (ANQ-ST). Complexation of those molecules with Pb^{2+} was studied at room temperature using UV-Visible absorption and fluorescence spectroscopies. Thanks to the UV-visible absorption spectroscopy, it appeared that ANQ-MMA formed 1:1 and 1:2 complexes with lead (II) and ANQ-ST only 1:1 complex. For both molecules, the fluorescence excitation-emission matrices (EEM) signal intensity increased from 0 to 100 $\mu mol.L^{-1}$ of lead (II) followed by a saturation for higher concentrations. The decomposition of the obtained EEMs gave a set of empiric fluorescent components that have been directly linked to the distribution of lead complexes obtained with the UV-visible absorption spectroscopy study. This correlation allowed to evidence metal/ligand complex stoichiometry and emerge as a new method to identify empiric components. Moreover, the two ligands showed a promising selectivity for Pb^{2+}, turning them interesting probes for this hazardous metal.

Keywords Metal/ligand complex · Spectroscopy · Modelling · Fluorescent molecules · Lead

Introduction

Lead is one of the most toxic metal for humankind and the environment. Lead naturally exists in Earth's crust but its presence in the environment is mainly due to human activities such as fuel combustion and industrial processes [1–3]. This trace metal can accumulate in water and soil organisms and influence the global balances and food chains [4]. Taken up from food, air or drinking water, lead causes inhibition of brain development, kidney and physical growth impairments [5, 6]. The maximum concentration level in drinking water is set at 10 $\mu g.L^{-1}$ [7]. The development of probes and sensors to detect lead therefore appears to be necessary especially for its most toxic species, the ionic lead (II) form. Fluorescence probes for the detection of trace metal ions is getting attention due to easy signal transduction and high sensitivity [8]. Fluorescent ligand for lead (II) have been recently developed based on fluorescein [9], rhodamine [10, 11], crown ether derivates [12, 13] or scaffold molecules [14–16].

Typical fluorescent chemosensors, also called fluoroionophores, include a recognition site or chelating group responsible for the efficiency of the binding and a fluorescent part that converts the ion recognition into a fluorescent signal. Upon ion complexation, their fluorescence response can be either quenched or enhanced but the turn-on response is preferable in order to avoid interferences with external factors that can be observed in the case of turn-off response [17]. One of the

---

Electronic supplementary material The online version of this article (https://doi.org/10.1007/s10895-019-02405-0) contains supplementary material, which is available to authorized users.

✉ Catherine Branger
branger@univ-tln.fr

✉ Véronique Lenoble
lenoble@univ-tln.fr

[1] MAPIEM Laboratory, University of Toulon, CS 60584, 83041 Toulon, Cedex 9, France

[2] IM2NP Laboratory, University of Toulon, CS 60584, 83041 Toulon, Cedex 9, France

[3] MIO Laboratory, University of Toulon, CS 60584, 83041 Toulon, Cedex 9, France

[4] Laboratory of Computational and Process Engineering, Lappeenranta-Lahti University of Technology LUT, P.O. Box 20, FI-53851 Lappeenranta, Finland

possible mechanism responsible for a turn-on fluorescence response is the photoinduced electron transfer (PET) process [18–20]. This process is based on a quenching of the fluorescence response of the fluorophore moiety by an electron transfer from the ionophore. Upon ion binding, this electron transfer is prevented and consequently fluorescence intensity is enhanced.

Anthracene is widely used as a fluorophore to design chemosensors, owing to the ease to modify its structure [21]. Anand et al. synthesized 5-((anthracen-9-ylmethylene)amino)quinoline-10-ol (ANQ), based on an anthracene platform, to detect lead (II) with a turn-on fluorescence response based on PET process [22]. In the present study, ANQ was modified in the para position of the imine group via a methoxy link to design two new fluorescent ligands for lead (II): (10-(8-hydroxyquinolin-5-ylimino)methyl)anthracen-9-yl)methyl methacrylate (ANQ-MMA) and ((10-((4-vinylbenzyloxy)methyl)anthracen-9-yl)methyleneamino)quinoline-8-ol (ANQ-ST). The formation of the complexes between lead (II) with ANQ-MMA and ANQ-ST was first investigated using UV-visible absorption spectroscopy and the distribution of the various complexes (1:1 complex, 1:2 complex,) as well as free metal and free ligand was calculated. In parallel, the fluorescence response of the two ligands upon the addition of lead (II) was analysed. Within this step, the recovered fluorescent signal was decomposed into a combination of fluorescent components. These components were then correlated to the above-mentioned possible 1:1 and 1:2 complexes. Such innovative correlation allowed to associate a modelled fluorescent signal with a complex of known-stoichiometry, an approach that opens a range of possibilities in the study of the interactions between ligand and metal ion.

Experimental

Reagents and Instruments

Anthraquinone, sodium hydride (60% in oil dispersion), lithium bromide, triethylamine, 4-vinylbenzylchloride, 18-crown-6 ether and 5-amino-8-hydroxyquinoline dihydrochloride were purchased from Sigma-Aldrich (reagent grade).

$AgNO_3$, $CaCO_3$, $ZnSO_4$ and $NaNO_3$ were purchased from Fisher Scientific (Analytical grade), $Al(NO_3)_3$, $CdSO_4$, $Co(NO_3)_2$ and $CuSO_4$ were from Merk (pro analysis grade), $Pb(NO_3)_2$ and $Fe(NO_3)_3$ were purchased from Carlo Erba (Analytical grade).

All other chemical reagents and solvents were purchased from Acros Organics (reagent grade). Dry solvents were purchased as extra dry grade (Acros Organics).

^{1}H, ^{13}C and ^{1}H - ^{13}C heteronuclear single quantum coherence (HSQC) nuclear magnetic resonance (NMR) measurements were obtained on a Bruker 400 MHz Ultrashield spectrometer.

Mass spectra were measured on a Bruker Esquire 6000 instrument.

Melting points were determined on a Bushi M-560 apparatus.

UV-visible absorption spectra were obtained with a Shimazu UV-2501 spectrometer.

Synthesis of (10-(8-Hydroxyquinolin-5-Ylimino) Methyl)Anthracen-9-Yl)Methyl Methacrylate (ANQ-MMA)

Step 3: Synthesis of (10-Formylanthracen-9-Yl)Methyl Methacrylate

2.51 mL of freshly distilled methacryloyl chloride (26 mmol) were added to a solution of 10-(hydroxymethyl)anthracen-9-carbaldehyde (3.04 g, 13 mmol) and triethylamine (10.76 mL, 77 mmol) in tetrahydrofuran cooled at 0 °C. The solution mixture was stirred at 0 °C for 2 h and then at room temperature for 20 h. The solvent was distilled off under reduced pressure. The crude product was solubilized in dichloromethane, washed five times with 100 mL of a saturated potassium carbonate solution and then twice with 100 mL of distilled water. The product was finally dried over magnesium sulphate to give 3.48 g of (10-formylanthracen-9-yl)methyl methacrylate. (Fig. 1a) Yield: 89%. Melting point: 132.7 °C.

^{1}H NMR (400 MHz, DMSO-d$_6$, δ in ppm), δ: 11.45 (s, 1H, CHO), 8.90 (dd, J = 7.6, 2.2 Hz, 2H, position 4), 8.54 (dd, J = 7.5, 2.1 Hz, 2H, position 7), 7.73 (m, 4H, position 5 and 6), 6.25 (s, 2H, CH_2), 5.94 (s, 1H, position 13), 5.63 (s, 1H, position 13), 1.83 (s, 3H, CH_3). (Online Resource, Fig. A).

^{13}C NMR (400 MHz, $CDCl_3$, δ in ppm), δ: 194.05 (C_{10}), 167.37 (C_{11}), 135.93 (C_2), 134.15 (C_{12}), 131.14(C_8), 130.66(C_3), 128.39(C_5), 127.74(C_9), 126.82 (C_6), 126.53 (C_{13}), 124.92 (C_7), 124.24 (C_4), 58.94 (C_1), 18.39 (C_{14}). (Online Resource, Fig. B).

LC-MS: calculated: 304. Found: 305.13 (*(10-formylanthracen-9-yl)methyl methacrylate* + H)$^+$ (Online Resource, Fig. C).

Step 4: Synthesis of (10-(8-Hydroxyquinolin-5-Ylimino) Methyl)Anthracen-9-Yl)Methyl Methacrylate (ANQ-MMA)

100 mL of an ethanolic solution containing (10-formylanthracen-9-yl)methyl-methacrylate (1.10 g, 3.62 mmol), 5-amino-8-hydroxyquinoline dihydrochloride (0.84 g, 3.62 mmol) and 5 drops of triethylamine was refluxed

for 4 h. Then the solvent was removed under reduced pressure. The crude product was washed with 100 mL of diethyl ether then with 100 mL of a solution containing potassium carbonate (0.55 g, 3.98 mmol) and extracted with dichloromethane. After distillation under reduced pressure, 1.21 g of the product ANQ-MMA is obtained. (Fig. 1b) Yield: 75%. Melting point: 220.0 °C.

^{1}H NMR (400 MHz, DMSO-d_6, δ in ppm), δ: 10.03 (s, 1H, OH), 9.96 (s, 1H, position 10), 8.95 (dd, J = 4.1, 1.6 Hz, 1H, position 15), 8.80 (d, J = 9.4 Hz, 2H, position 4), 8.73 (dd, J = 8.5, 1.6 Hz, 1H, position 14), 8.54 (d, J = 8.2 Hz, 2H, position 7), 7.78 (d, J = 8.2 Hz, 1H, position 13), 7.67 (m, 5H, position 5, 6 and 19), 7.25(d, 1H, position 18), 6.30 (s, 2H, CH_2), 5.96 (s, 1H, position 22), 5.65 (s, 1H, position 22), 1.86 (s, 3H, CH_3). (Online Resource, Fig. D).

^{13}C NMR (400 MHz, DMSO-d_6, δ in ppm), δ: 167.05 (C_{20}), 159.14 (C_{10}), 153.24 (C_{17}), 149.26 (C_{15}), 139.58, 138.92, 136.23, 132.80, 130.70, 130.18, 130.01, 127.29, 126.79, 126.30, 125.26, 122.65, 115.34 (C_{18}), 111.81 (C_{19}), 59.39 (C_1), 18.55 (C_{23}). (Online Resource, Fig. E).

LC-MS: calculated: 446. Found: 447.14 (*ANQ-MMA* + H^+) (Online Resource, Fig. F).

Two new chemosensors for lead (II) were synthesized based on 5-((anthracen-9-ylmethylene) amino)quinolin-10-ol (ANQ). ANQ was modified in the para position of the imine group via a methoxy link either with methylmethacrylate (ANQ-MMA) or styrene (ANQ-ST). Complexation of those molecules with Pb^{2+} was studied at room temperature using UV-Visible absorption and fluorescence spectroscopies. Thanks to the UV-visible absorption spectroscopy, it appeared that ANQ-MMA formed 1:1 and 1:2 complexes with lead (II) and ANQ-ST only 1:1 complex. For both molecules, the fluorescence excitation-emission matrices (EEM) signal intensity increased from 0 to 100 μmol.L-1 of lead (II) followed by a saturation for higher concentrations. The decomposition of the obtained EEMs gave a set of empiric fluorescent components that have been directly linked to the distribution of lead complexes obtained with the UV-visible absorption spectroscopy study. This correlation allowed to evidence metal/ligand complex stoichiometry and emerge as a new method to identify empiric components. Moreover, the two ligands showed a promising selectivity for Pb^{2+}, turning them interesting probes for this hazardous metal.

Synthesis of ((10-((4-Vinylbenzyloxy)Methyl) Anthracene-9-Yl)Methyleneamino)Quinoline-8-Ol (ANQ-ST)

Synthesis of 4-Vinylbenzyliodide

This synthesis was inspired from Chalal et al. work [23]. A mixture of 4-vinylbenzylchloride (5.0 g, 32.9 mmol) and NaI (7.0 g, 42.7 mmol) in acetone under argon was refluxed for 20 h. After cooling, the mixture was poured into water and extracted with dichloromethane. To neutralize the excess of iodine, the mixture was washed twice with 100 mL of Na_2SO_3 saturated solution. Then, the organic phase was washed twice with 100 mL of water and dried over magnesium sulphate. After removal of the solvent under reduced pressure, 7,9 g of product was obtained. (Fig. 2a) Yield: 99%.

^{1}H NMR (400 MHz, $CDCl_3$, δ in ppm), δ: 7.38 (s, 4H, aromatic H), 6.74 (dd, J = 17.6, 10,7 Hz, 1H, position 6), 5.82 (dd, J = 17.6, 0.7 Hz, 1H, position 7), 5.32 (dd, 10.7, 0.7 Hz, 1H, position 7), 4.50 (s, 2H, position 1). (Online Resource, Fig. G).

^{13}C NMR (400 MHz, $CDCl_3$, δ in ppm), δ: 138.95 (C_2), 137.32 (C_5), 136.39 (C_6), 129.13 (C_3), 126.81 (C_4), 114.58 (C_7), 6.09 (C_1). (Online Resource, Fig. H).

^{1}H - ^{13}C HSQC NMR (400 MHz, $CDCl_3$): Expected crosspeaks signals were observed. (Online Resource, Fig. I).

Step 3′: Synthesis of 9-((4-Vinylbenzyloxy)Methyl) Anthracene-10-Carbaldehyde

In a 250 mL flask, 287 mg of sodium hydride (7.2 mmol), 35 mg of 18-crown-6 ether and 10 mL of dry tetrahydrofuran were added. The mixture was put under argon and cooled down with a water/ice bath. Then 1.00 g of 10-(hydroxymethyl)anthracen-9-carbaldehyde (4.23 mmol) dissolved in 100 mL of dry tetrahydrofuran were slowly added. After one hour of stirring at room temperature and under argon, the mixture was cooled with a water/ice bath and 1,76 g of 4-vinylbenzyliodide (7.2 mmol) diluted in 10 mL of dry tetrahydrofuran was added dropwise. The mixture was stirred for 24 h under argon at room temperature, then a few drops of water were added and the tetrahydrofuran was distilled off under reduced pressure. The crude product was extracted with dichloromethane and dried over magnesium sulphate. The dichloromethane was distilled off under reduced pressure to give a residue which was washed twice with 50 mL of cold hexane and purified on a silica gel column eluting with ethyl acetate–cyclohexane (1:9, *v*/v) to obtain 490 mg of the product as a yellow oil. (Fig. 2b) Yield: 33%.

^{1}H NMR (400 MHz, $CDCl_3$, δ in ppm), δ: 11.46 (s, 1H, CHO), 8.87 (d, J = 8.8 Hz, 2H, position 13), 8.36 (d, J = 8.8 Hz, 2H, position 14), 7.61 (dtd, 4H, positions 4 and 7), 7.42 (dd, 4H, positions 5 and 6), 6.78 (dd, J = 17.6, 10.9 Hz, 1H, position 16), 5.82 (dd, J = 17.6, 0.8 Hz, 1H, CH_2), 5.42 (s, 2H, position 1), 5.31 (dd, J = 10.9, 0.8 Hz, 1H, CH_2), 4.73 (s, 2H, position 11). (Online Resource, Fig. J).

^{13}C NMR (400 MHz, $CDCl_3$, δ in ppm), δ: 193.96 (C_{10}), 137.57 (C_2), 137.45 (C_{15}), 136.75 (C_{12}), 136.60 (C_{16}), 131.28 (C_8), 130.53 (C_9), 128.45 (C_5), 128.33 (C_6), 126.82 (C_3), 126.46 (C_7), 126.36 (C_4), 125.23 (C_{14}), 124.07 (C_{13}), 114.18 (C_{17}), 72.71 (C_{11}), 64.05 (C_1). (Online Resource, Fig. K).

^1H - ^{13}C HSQC NMR (400 MHz, $CDCl_3$): Expected crosspeaks signals were observed. (Online Resource, Fig. L).

Step 4′: Synthesis of ((10-((4-Vinylbenzyloxy)Methyl) Anthracen-9-Yl)Methyleneamino)Quinoline-8-Ol (ANQ-ST)

100 mL of an ethanolic solution containing 9-((4-vinylbenzyloxy)methyl)antharcene-10-carbaldehyde (380 mg, 1.08 mmol), 5-amino-8-hydroxyquinoline dihydrochloride (252 mg, 1.08 mmol) and 10 drops of triethylamine was refluxed for 4 h. Then the solvent was removed under reduced pressure and the crude product was washed twice with 100 mL of diethyl ether. After distillation under reduced pressure of the filtrate, the product was chromatographed on silica gel 60 eluting with ethyl acetate–cyclohexane (1:9, *v*/v). Evaporation of the appropriate fractions gave 160 mg of ANQ-ST, as brown powder. (Fig. 2c) Yield: 30%. Melting point: 210 °C.

^1H NMR (400 MHz, $CDCl_3$, δ in ppm), δ: 9.84 (s, 1H, position 10, 8.89 (dd, J = 4.2, 1.6 Hz, 1H, position 15) 8.85 (dd, j = 8.5, 1.6 Hz, 1H, position 13), 8.78 (m, 2H, position 22), 8.44 (m, 2H, position 23), 7.60 (m, 4H, positions 4 and 7), 7.52 (dd, J = 8.5, 4.5 Hz, 1H, position 14), 7.44 (m, 5H, positions 5, 6 and 19), 7.31 (m, 1H, position 18), 6.77 (dd, J = 17.6, 10.9 Hz, 1H, position 25), 5.80 (dd, J = 17.6, 0.8 Hz, 1H, CH_2), 5.57 (s, 2H, position 1), 5.29 (dd, J = 10.9, 0.8 Hz, 1H, CH_2), 4.76 (s, 2H, position 20). (Online Resource, Fig. M).

^{13}C NMR (400 MHz, $CDCl_3$, δ in ppm), δ: 158.84 (C_{10}), 151.33(C_{17}), 148.59 (C_{15}), 140.88 (C_{11}), 138.33 (C_{16}), 137.87 (C_2), 137.35 (C_{21}), 136.64 (C_{25}), 133.48 (C_{13}), 132.39 (C_{24}), 130.90 (C_9), 130.34 (C_8), 129.69 (C_3), 128.38 (C_5), 126.67 (C_6), 126.41 (C_7), 126.22 (C_4), 125.52 (C_{22}), 125.19 (C_{12}), 124.14 (C_{23}), 122.00 (C_{14}), 114.02 (C_{19}), 113.94 (C_{26}), 109.72 (C_8), 72.38 (C_{20}), 64.20 (C_1). (Online Resource, Fig. N).

LC-MS: calculated: 494. Found: 495.18 (*ANQ-ST* + H^+) (Online Resource, Fig. O).

^1H -^{13}C HSQC NMR (400 MHz, $CDCl_3$): Expected crosspeaks signals were observed. (Online Resource, Fig. P).

Lead (II) and ANQ-MMA or ANQ-ST Species Distribution Modelling from UV-Visible Spectra

Lead (II) complexation by ANQ-MMA and ANQ-ST was studied in acetone (80%) - water (20%) mixture at room temperature. The experiments were performed in 3 mL quartz Suprasil cells. The combined concentration of lead (II) (0.01–0.09 $mmol.L^{-1}$) and ANQ-MMA or ANQ-ST (0.09–0.01 $mmol.L^{-1}$) was kept constant (0.1 $mmol.L^{-1}$), but the ratio ligand/lead was varied from 0.1 to 10 using $Pb(NO_3)_2$ as lead source. For the two molecules, 14 spectra were recorded using UV-vis spectrometer.

At equilibrium, the distribution of the various species (free metal, 1:1 complex, 1:2 complex and free ligand) was calculated using a commercial program (HypSpec) based on the least-squares minimization scheme [24, 25]. Stability constants, extinction coefficients and concentrations of all absorbing components were simultaneously estimated. For uncomplexed lead (II), the extinction coefficients were calculated from independent measurements.

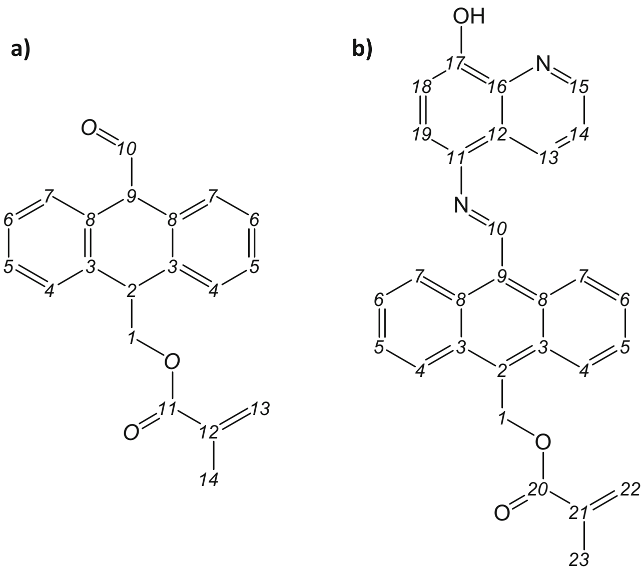

Fig. 1 Indexation of the carbons observed on the ^{13}C NMR spectrum of a) (10-formylanthracen-9-yl)methyl methacrylate and b) ANQ-MMA

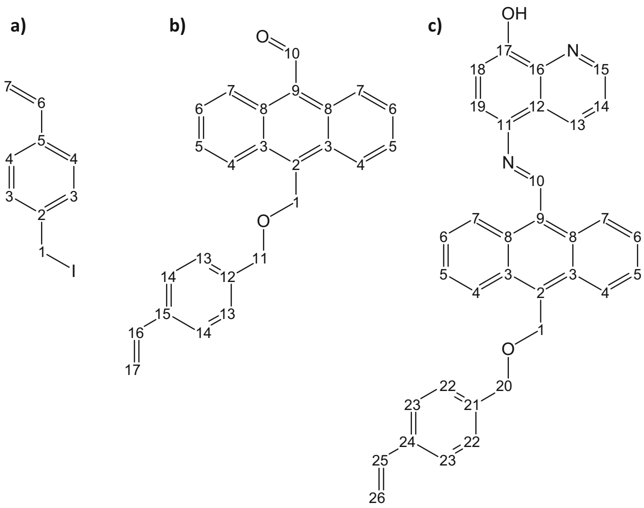

Fig. 2 Indexation of the carbons observed on the ^{13}C NMR spectrum of a) 4-vinylbenzyliodide, b) 9-((4-vinylbenzyloxy)methyl)anthracene-10-carbaldehyde and c) ANQ-ST

Fluorescence Measurements

Lead Experiments

All experiments and measurements were performed at room temperature, in acetone (80%) - water (20%) mixture. $AgNO_3$, $CaCO_3$, $NaNO_3$, $CdSO_4$, $Co(NO_3)_2$, $CuSO_4$, $Pb(NO_3)_2$, $ZnSO_4$ $Al(NO_3)_3$, and $Fe(NO_3)_3$ were used as metal sources.

The fluorescent signal as a function of increasing lead concentration was studied. Solutions containing 50 $\mu mol.L^{-1}$ of the fluoroionophore ANQ-MMA or ANQ-ST and 0, 5,10, 30, 50, 100 and 300 $\mu mol.L^{-1}$ of lead (II) were prepared and analysed.

The fluorescence signal of each the two synthesized molecules in presence of lead or other ions, taken separately, was measured. Solutions containing 50 $\mu mol.L^{-1}$ of the molecule and 200 $\mu mol.L^{-1}$ of lead (II) or 200 $\mu mol.L^{-1}$ of silver (I), sodium (I), calcium (II), cadmium (II), cobalt (II), copper (II), zinc (II), aluminium (III) or iron (III) were prepared and analysed for their fluorescence signal.

Then, the fluorescent signal of a constant lead concentration in presence of interfering ions was studied. A solution containing 50 $\mu mol.L^{-1}$ fluoroionophore, 100 $\mu mol.L^{-1}$ of lead and 100 $\mu mol.L^{-1}$ of one interfering ion was prepared. The interfering ion was chosen among silver (I), sodium (I), calcium (II), cadmium (II), cobalt (II), copper (II), zinc (II), aluminium (III) or iron (III).

Excitation-Emission Matrix (EEM) of Fluorescence Measurement

The EEMs were measured on a HITACHI F4500 spectrofluorimeter. The excitation wavelength ranged from 320 to 460 nm, with a step of 10 nm and an excitation slit of 1 nm. The corresponding emission spectra were acquired from 350 to 550 nm with a scan speed of 2400 $nm.min^{-1}$ and a slit of 1 nm. The photomultiplicator tension was fixed at 950 V and the integration time set at 0.1 s. The extraction of the 5 nm stepped emission was obtained by FL-Solution software.

CP/PARAFAC Analysis

First, all the EEMs were cleaned from the diffusion signals: Rayleigh by cutting the diffusion band (20 nm) and Raman from first and second order by applying Zepp procedure [26]. Then, CP/PARAFAC algorithm was used [27, 28]. This algorithm allows the decomposition of a dataset of matrices into a set of fluorescent components, considering that all the considered EEM are constituted by a linear combination of the same independent components. The correct number of components needed to model the dataset is defined by evaluating the CORCONDIA score. Users have to test a range of model, i.e. number of components, to detect the best number of components [29]. In this work, decomposition investigation was done from two to five components and the higher number of component giving a CORCONDIA test over

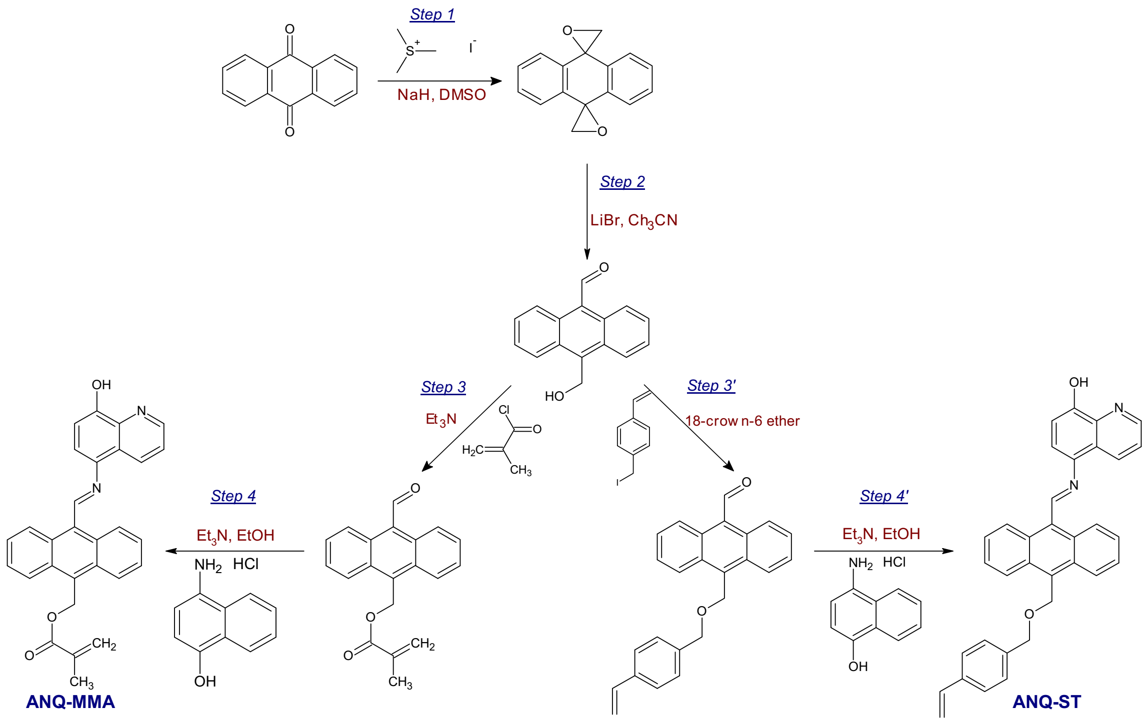

Fig. 3 Synthesis route of ANQ-MMA and ANQ-ST

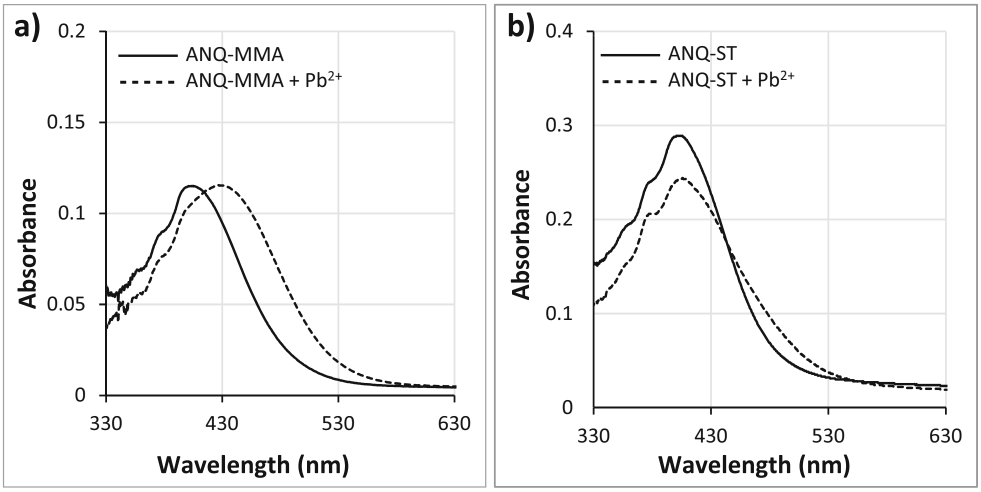

Fig. 4 Absorbance spectra of (**a**) ANQ-MMA and (**b**) ANQ-ST (50 µmol.L^{-1}) in acetone-water (4:1, *v*/v) solution and in presence of 100 µmol.L^{-1} of Pb^{2+}

60% was selected as the optimal component number [30]. Then some components given by this decomposition were directly linked to the complexes metal-ligand evidenced by the UV-visible study.

Results and Discussions

Synthesis and Properties of Fluoroionophores ANQ-MMA and ANQ-ST

The synthesis of ANQ-MMA and ANQ-ST took place in four steps with an overall yield of 63% for ANQ-MMA and 10% for ANQ-ST (Fig. 3). For both fluoroionophores, the first two steps were inspired by the work of various authors [31–34]. They enable the functionalization of anthracene in the para position of the future imine group. For ANQ-MMA, the third step is an esterification reaction catalysed by a tertiary amine, followed by a coupling between the intermediate compound and the 5-amino-8-hydroxyquinoline dihydrochloride. In order to synthesize ANQ-ST, the intermediate compound, 4-vinylbenzyliodide, was prepared to couple 10-(hydroxymethyl)anthracen-9-carbaldehyde by its hydroxyl group with 4-vinylbenzyle before the final Schiff-base formation reaction. Molecular structures were characterized by ^{1}H NMR, ^{13}C NMR, ^{1}H-^{13}C HSQC NMR and LC-MS techniques (see Experimental section).

The photophysical properties of ANQ-MMA and ANQ-ST were investigated. Both molecules showed a major absorption band at 405 nm. Upon addition of Pb^{2+}, the absorbance of ANQ-MMA (Fig. 4a) and ANQ-ST (Fig. 4b) underwent a red shift of 25 and 3 nm respectively. This result emphasized a photophysical effect of lead (II) complexation by those molecules.

Complex formation was studied by keeping the overall concentration of lead and fluoroionophore constant while varying their molar ratio. The distribution of the complexes formed between Pb^{2+} and the two fluoroionophores was calculated using HypSpec, a commercial program, based on the least squares minimization method (Fig. 5) [24], using the following equilibrium equations:

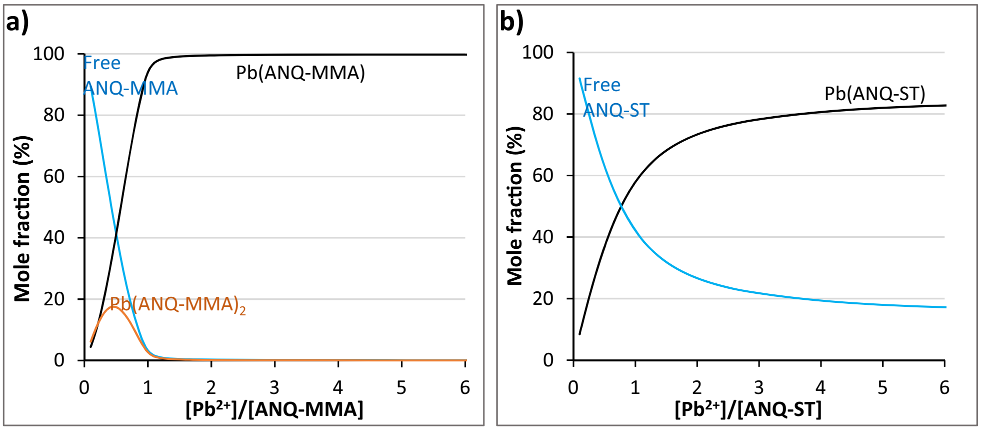

Fig. 5 Metal and ligand species distribution calculated from UV-vis spectra using HypSpec program [25] for lead and (**a**) ANQ-MMA or (**b**) ANQ-ST. Solvent: acetone-water (4:1, v/v)

Table 1 Stability constants of the complexes formed with lead for ANQ-MMA and ANQ-ST

	Log (β_1)	Log (β_2)
ANQ-MMA	7.2	11.8
ANQ-ST	5.1	/

$$M + L \Leftrightarrow ML \text{ with } K_{ML} = \frac{[ML]}{[M].[L]}$$

$$ML + L \Leftrightarrow ML_2 \text{ with } K_{ML_2} = \frac{[ML_2]}{[ML].[L]}$$

$$[L]_0 = [L] + [ML] + 2[ML_2]$$

$$[M]_0 = [M] + [ML] + [ML_2]$$

The amount of each complex is given as a fraction of the total distribution and stability constants in Table 1. According to the distribution diagrams, for ANQ-MMA, 1:1 and 1:2 complexes coexist up to a ratio of 1 between Pb^{2+} and ANQ-MMA, then only the 1:1 remains in solution. For ANQ-ST, whatever the ratio used, only the 1:1 complex is formed in solution. Stability constants values proved that the formation of all the complexes is quantitative with a higher Log (β1) value for ANQ-MMA.

Fluorescent Detection of Pb^{2+}

The fluorescence of the molecules was monitored upon the addition of lead (II). The EEMs showed a massive peak located at ($\lambda_{ex}/\lambda_{em}$) = 388/425 nm for ANQ-MMA (Fig. 6) and at ($\lambda_{ex}/\lambda_{em}$) = 380/420 nm for ANQ-ST (Fig. 7). For both molecules, the relative peak intensity of the EEMs underwent an important increase from 0 to 100 µmol.L^{-1} of lead (II) followed by a saturation for higher concentrations (Fig. 8).

For ANQ-ST ligand, PARAFAC treatment gave optimum results for two components (CORCONDIA = 94%). CORCONDIA scores obtained for 2 to 5 components decomposition are given in Table A (Online Resource). Component 1 showed a maximum located at $\lambda_{ex}/\lambda_{em}$ = 385–405/430–440 nm. Component 2 showed a maximum located at $\lambda_{ex}/\lambda_{em}$ = 370–385/405–420 nm (Fig. 9a). Once those components extracted, the contribution to fluorescence of each component to each EEM was calculated (Fig. 9b). Each component fluorescence contribution is proportional to their concentration and to a quantum yield of fluorescence [35]. Coupling PARAFAC decomposition with the species distribution (see section 3.1), it seemed difficult to directly linked an empiric component to species with known stoichiometry. Indeed, the two empiric components given by the decomposition had the same contribution evolution. Correlating components contribution to Pb(ANQ-ST) complex concentration, both components had a good correlation with the formed complex (Fig. 9c). In other terms, it appeared that PARAFAC decomposition was not able to identify and separate real substances. It was probably because of the too close fluorescence ranges of the real species. Indeed, a small 3 nm red-shift was observed on the absorbance spectra when lead (II) was added to ANQ-ST (Fig. 4) meaning that free ANQ-ST and complexed ANQ-ST have probably close fluorescence ranges.

For ANQ-MMA ligand, PARAFAC treatment decomposition gave an optimum result for three components (CORCONDIA = 77%). CORCONDIA scores obtained for 2 to 5 components decomposition are given in Table A. Component 1 presented an excitation wavelength maximum at 365–385 nm and emission maximum at 420–440 nm. Component 2 presented an excitation wavelength maximum at 385–400 nm and emission maximum at 495–505 nm. Component 3 showed two maxima: one located at $\lambda_{ex}/\lambda_{em}$ = 410/450 nm and the other one located at $\lambda_{ex}/\lambda_{em}$ = 345–350/

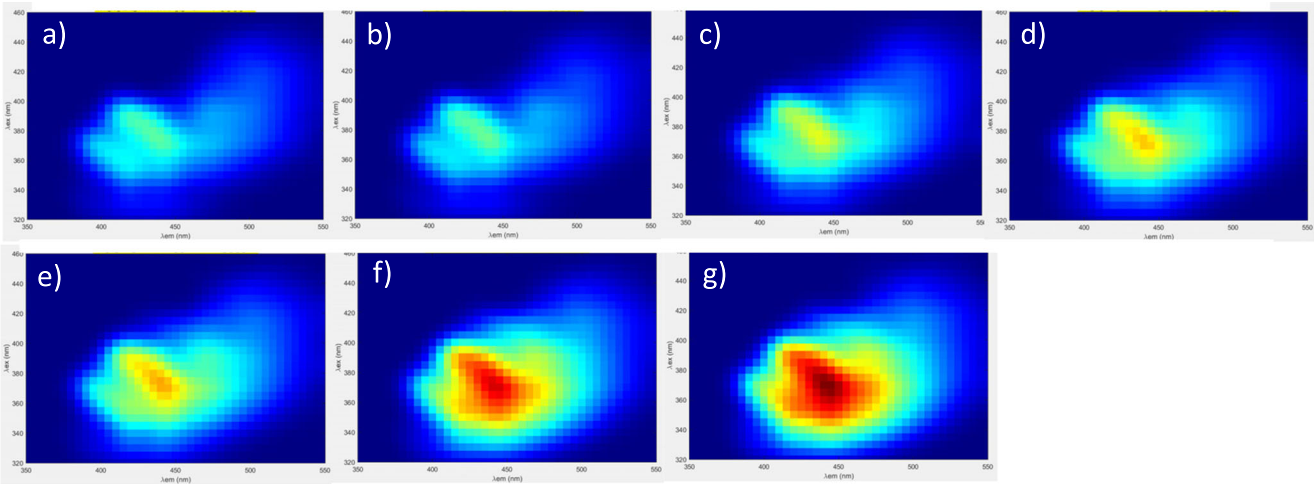

Fig. 6 EEMs obtained for acetone-water (4:1, v/v) solutions containing 50 µmol.L^{-1} of ANQ-MMA and (**a**) 0, (**b**) 5, (**c**) 10, (**d**) 30, (**e**) 50, (**f**) 100 or (**g**) 300 µmol.L^{-1} of Pb^{2+}

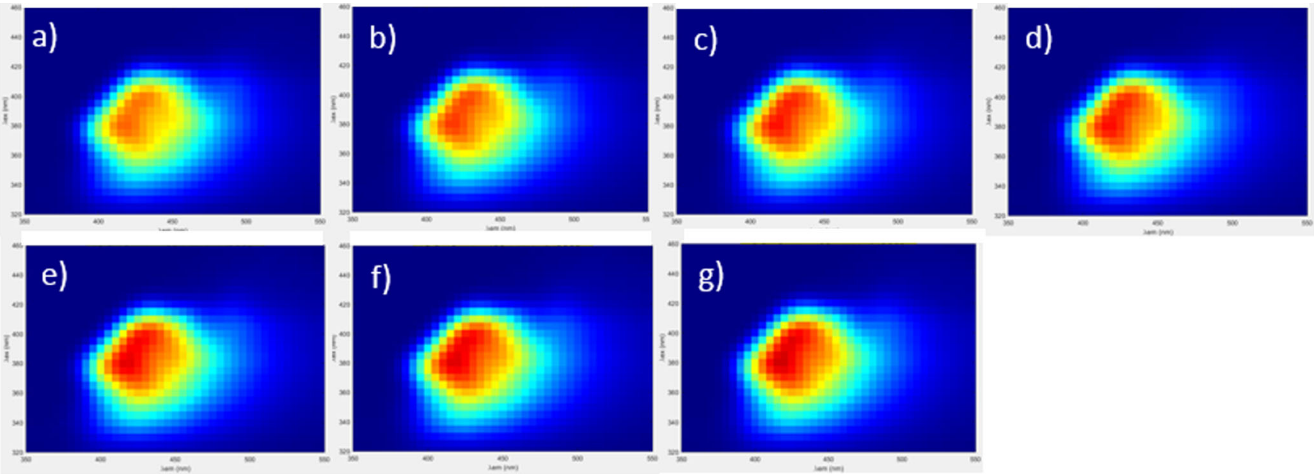

Fig. 7 EEMs obtained for acetone-water (4:1, v/v) mixtures solutions containing 50 µmol.L^{-1} of ANQ-ST and (**a**) 0, (**b**) 5, (**c**) 10, (**d**) 30, (**e**) 50, (**f**) 100 or (**g**) 300 µmol.L^{-1} of Pb^{2+}

445–455 nm (Fig. 10a). The contribution of each component to each EEM measurements is depicted in Fig. 10b. Coupling PARAFAC decomposition with the species distribution (see section 3.1), it was possible to discriminate the 3 PARAFAC components, compared to species of known stoichiometry. Looking at the components contribution, it was clear that none of them presented the variation corresponding to Pb(ANQ-MMA)$_2$ (Fig. 5). Furthermore, no correlation could be pointed out for this complex (Fig. 10c). On another hand, components 1 and 3 could be linked to Pb(ANQ-MMA), looking at their correlation (Fig. 10d). Yet, two arguments clearly led to the conclusion that component 3 is directly linked to the predominant complex Pb(ANQ-MMA). First, component 3 concentration is increasing starting from zero, unlike component 1. Then, the comparison of the maximum excitation wavelengths observed in these components EEM (Fig. 10a) with the 25 nm red-shift observed on absorbance spectra when lead (II) was added to ANQ-MMA (Fig. 1) indicated that component 3 was more likely to be associated to Pb(ANQ-MMA) complex. For ANQ-MMA, it was therefore possible to link the fluorescent modelled component to an existing complex and to further demonstrate its stoichiometry.

Competition Analysis

The fluorescence properties of ANQ-MMA and ANQ-ST were measured in presence of different metal ions. Results showed that both fluoroionophores could almost selectively recognize Pb^{2+} via fluorescence "off-on" responses. Indeed, an exaltation of the fluorescence intensity on the EEMs was observed only when Pb^{2+} was added to ANQ-MMA or ANQ-ST. For ANQ-MMA, a fluorescent signal was also recorded in

Fig. 8 Relative fluorescence intensity of acetone/water (4:1, v/v) solutions containing 50 µmol.L^{-1} of (**a**) ANQ-MMA or (**b**) ANQ-ST upon the addition of lead ion

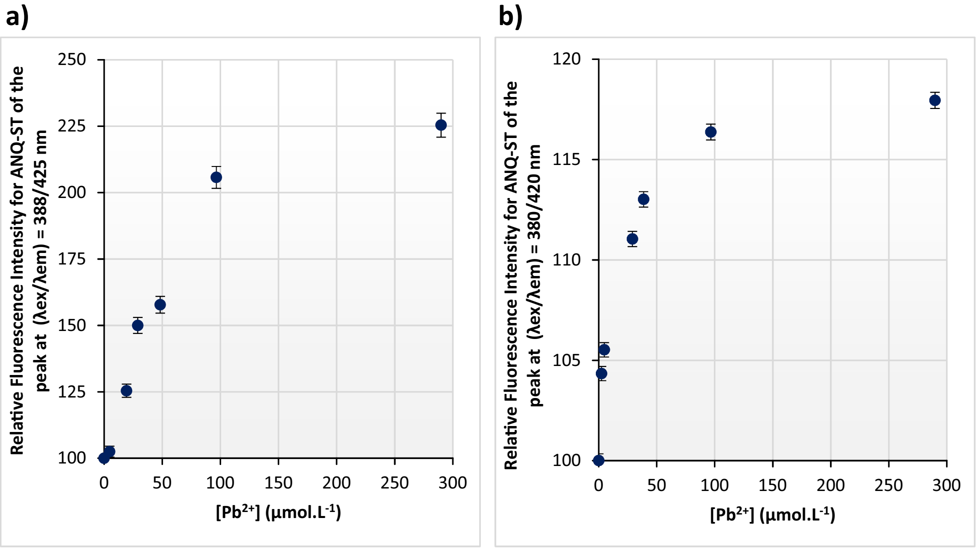

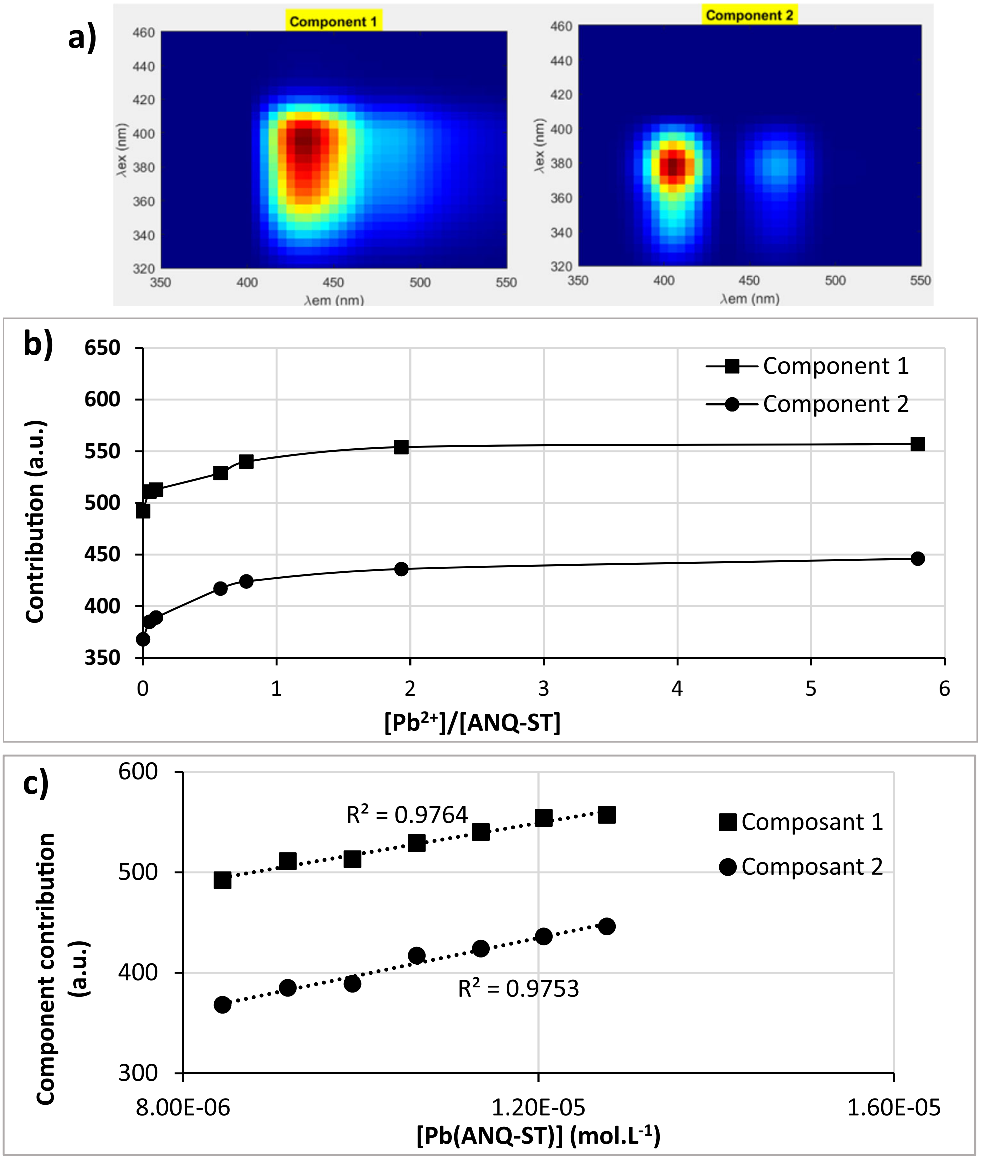

Fig. 9 (**a**) Component 1 and 2 obtained with PARAFAC decomposition with an optimum CORCONDIA score, (**b**) their contribution to fluorescence for ANQ-ST lead range study and (**c**) their contribution correlated to Pb(ANQ-ST) concentration as calculated in Fig. 2

presence of Na^+ (Online Resource, Fig. Q) and for ANQ-ST in presence of Co^{2+} (Online Resource, Fig. R) but the extent of the measured fluorescence was clearly below that obtained in presence of Pb^{2+}.

To determine the effect of other metal ions on the selectivity of ANQ-MMA and ANQ-ST for Pb^{2+}, competition experiments were carried out by measuring the fluorescence behaviour of the molecules in presence of Pb^{2+} ions and another metal ion (Ag^+, Na^+, Ca^{2+}, Cd^{2+}, Co^{2+}, Cu^{2+}, Zn^{2+}, Al^{3+} or Fe^{3+}) (Online Resource, Fig. S and Fig. T). As seen in Fig. 11, for both molecules, all solutions containing an interfering ion, except for Fe^{3+}, showed very weak variation of fluorescence intensity compared to the fluorescence intensity of the solution containing lead (II). These results demonstrate that ANQ-MMA and ANQ-ST can act as selective probes for fluorescence detection of Pb^{2+}.

Conclusion

Two fluorescent ligands specific to lead (II) were synthesized: ANQ-MMA and ANQ-ST. Their turn-on fluorescence response upon the addition of Pb^{2+} was studied. The decomposition of the fluorescence excitation-emission matrices allowed to give the number of fluorescent components involved in the fluorescent signal. The coupling of those results with the complex distribution of ANQ-MMA and ANQ-ST with lead (II) established by a UV-visible study allowed to link

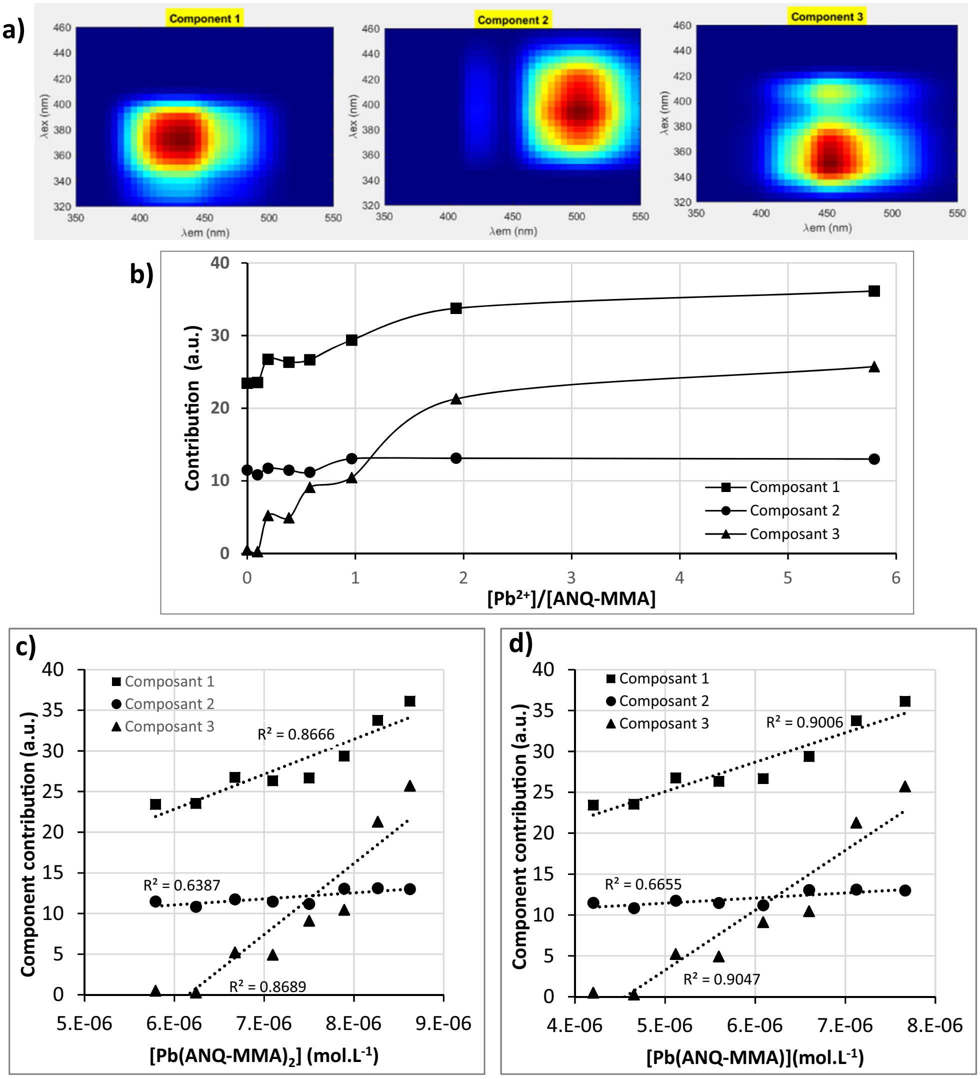

Fig. 10 (**a**) Component 1, 2 and 3 obtained with PARAFAC decomposition with an optimum CORCONDIA score and (**b**) their contribution to fluorescence for ANQ-MMA lead range study and their contribution correlated to (**c**) Pb(ANQ-MMA)$_2$ and (**d**) Pb(ANQ-MMA) concentration as calculated in Fig. 2

a modelled fluorescent component to a real complex of a known stoichiometry. Comparing fluorescence decomposition and UV-visible study appeared to be a new promising way to identify species. Moreover, the two synthesized ligands showed interesting properties which could turn them as interesting probes, specific for lead (II). As a matter of fact, in addition to their turn-on fluorescence responses upon the addition of lead (II),

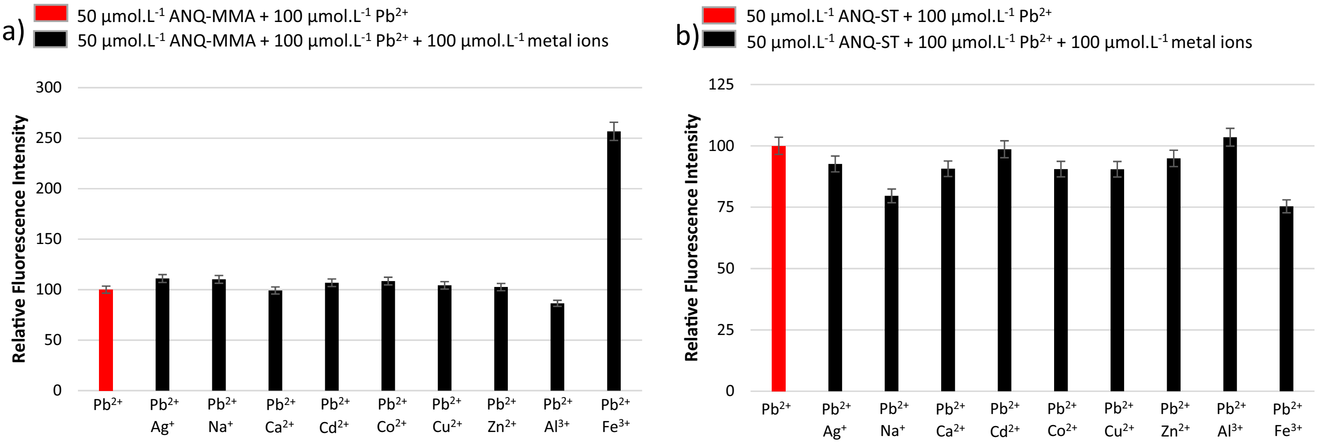

Fig. 11 Competition analysis of (**a**) ANQ-MMA and (**b**) ANQ-ST (50 µmol.L-1) in acetone-water (4:1, *v*/v) at room temperature

the performed competition analysis demonstrated their selectivity.

Acknowledgements This work is part of the PREVENT program financed by the University of Toulon, Toulon-Provence-Méditerranée and the Conseil Départemental du Var, France. The authors acknowledge financial support from the Regional Council of Provence Alpes Côte d'Azur (France) and Academy of Finland.

References

1. Kim HN, Ren WX, Kim JS, Yoon J (Mar. 2012) Fluorescent and colorimetric sensors for detection of lead, cadmium, and mercury ions. Chem Soc Rev 41(8):3210–3244
2. Chen C-T, Huang W-P (Jun. 2002) A Highly Selective Fluorescent Chemosensor for Lead Ions. J Am Chem Soc 124(22):6246–6247
3. Flegal AR, Smith DR (Jun. 1992) Current needs for increased accuracy and precision in measurements of low levels of lead in blood. Environ Res 58(1):125–133
4. Wierzbicka M, Antosiewicz D (Jan. 1993) How lead can easily enter the food chain — a study of plant roots. Sci Total Environ 134:423–429
5. Wang L, Jin Y, Deng J, Chen G (Nov. 2011) Gold nanorods-based FRET assay for sensitive detection of Pb2+ using 8-17DNAzyme. Analyst 136(24):5169–5174
6. Wei Y, Liu R, Wang Y, Zhao Y, Cai Z, Gao X (Mar. 2013) Hairpin oligonucleotides anchored terbium ion: a fluorescent probe to specifically detect lead(II) at sub-nM levels. Analyst 138(8):2302–2307
7. The European Union (1998) Council Directive 98/83/EC of 3 November 1998 on the quality of water intended for human consumption. Off J Eur Communities, vol L 330:32–54, Dec
8. Y. Chen and K. Wang, Azacrown[N,S,O]-modified porphyrin sensor for detection of Ag+, Pb2+, and Cu2+. Photochem Photobiol Sci, vol. 12, no. 11, pp. 2001–2007, Oct. 2013.
9. Zheng H, Zhan X-Q, Bian Q-N, Zhang X-J (2012) Advances in modifying fluorescein and rhodamine fluorophores as fluorescent chemosensors. Chem Commun 49(5):429–447, Dec
10. A. Pal, B. Bag, M. Thirunavoukkarasu, S. Pattanaik, and B. K. Mishra, Solvent mediated tuning of selectivity in a rhodamine based probe and bioimaging for Pb(II) detection in plant tissues. RSC Adv, vol. 3, no. 40, pp. 18263–18266, Sep. 2013.
11. Sunnapu O, Kotla NG, Maddiboyina B, Singaravadivel S, Sivaraman G (2015) A rhodamine based 'turn-on' fluorescent probe for Pb(II) and live cell imaging. RSC Adv 6(1):656–660, Dec
12. Xia W-S, Schmehl RH, Li C-J, Mague JT, Luo C-P, Guldi DM (Jan. 2002) Chemosensors for Lead(II) and Alkali Metal Ions Based on Self-Assembling Fluorescence Enhancement (SAFE). J Phys Chem B 106(4):833–843
13. Park J, Kim Y (Jun. 2012) A colorimetric probe for the selective naked-eye detection of Pb(II) ions in aqueous media. Analyst 137(14):3246–3248
14. Chen Y, Jiang J (Jun. 2012) Porphyrin-based multi-signal chemosensors for Pb2+ and Cu2+. Org Biomol Chem 10(24):4782–4787
15. Pandey R, Gupta RK, Shahid M, Maiti B, Misra A, Pandey DS (Jan. 2012) Synthesis and Characterization of Electroactive Ferrocene Derivatives: Ferrocenylimidazoquinazoline as a Multichannel Chemosensor Selectively for Hg2+ and Pb2+ Ions in an Aqueous Environment. Inorg Chem 51(1):298–311
16. Goswami S, Chakrabarty R (Jul. 2010) Highly Selective Colorimetric Fluorescent Sensor for Pb2+. Eur J Org Chem 2010(20):3791–3795
17. Valeur B, Berberan-Santos MN (2012) Molecular Fluorescence: Principles and Applications. John Wiley & Sons
18. Valeur B, Leray I Design principles of fluorescent molecular sensors for cation recognition. Coord Chem Rev 205(1):3–40 août 2000
19. Liu Z, He W, Guo Z (Jan. 2013) Metal coordination in photoluminescent sensing. Chem Soc Rev 42(4):1568–1600
20. de Silva AP et al (Aug. 1997) Signaling Recognition Events with Fluorescent Sensors and Switches. Chem Rev 97(5):1515–1566
21. Jun EJ, Swamy KMK, Bang H, Kim S-J, Yoon J (May 2006) Anthracene derivatives bearing thiourea group as fluoride selective fluorescent and colorimetric chemosensors. Tetrahedron Lett 47(18):3103–3106
22. Anand T, Sivaraman G, Mahesh A, Chellappa D (Jan. 2015) Aminoquinoline based highly sensitive fluorescent sensor for lead(II) and aluminum(III) and its application in live cell imaging. Anal Chim Acta 853:596–601
23. Chalal M, Vervandier-Fasseur D, Meunier P, Cattey H, Hierso J-C (May 2012) Syntheses of polyfunctionalized resveratrol derivatives using Wittig and Heck protocols. Tetrahedron 68(20):3899–3907
24. Laatikainen M et al (Jul. 2014) Complexation of Nickel with 2-(Aminomethyl)pyridine at High Zinc Concentrations or in a Nonaqueous Solvent Mixture. J Chem Eng Data 59(7):2207–2214
25. Gans P, Sabatini A, Vacca A (1985) SUPERQUAD: an improved general program for computation of formation constants from potentiometric data. J Chem Soc Dalton Trans 0(6):1195–1200
26. Zepp RG, Sheldon WM, Moran MA (Oct. 2004) Dissolved organic fluorophores in southeastern US coastal waters: correction method for eliminating Rayleigh and Raman scattering peaks in excitation–emission matrices. Mar Chem 89(1):15–36
27. Bro R (Oct. 1997) PARAFAC. Tutorial and applications. Chemom Intell Lab Syst 38(2):149–171
28. Stedmon CA, Markager S (Mar. 2005) Resolving the variability in dissolved organic matter fluorescence in a temperate estuary and its catchment using PARAFAC analysis. Limnol Oceanogr 50(2):686–697
29. Bro R, Kiers HAL (Jun. 2003) A new efficient method for determining the number of components in PARAFAC models. J Chemom 17(5):274–286
30. Mounier S, Zhao H, Garnier C, Redon R (Oct. 2011) Copper complexing properties of dissolved organic matter: PARAFAC treatment of fluorescence quenching. Biogeochemistry 106(1): 107–116
31. Mahmoodi NO, Mirkhaef S, Ghavidast A (2015) Synthesis of anthracene derivatives of 1,3-diazabicyclo[3.1.0]hex-3-ene. J Mol Struct 1081:248–253, février
32. Yu M, He F, Tang Y, Wang S, Li Y, Zhu D (Jun. 2007) Non-Ionic Water-Soluble Crown-Ether-Substituted Polyfluorene as Fluorescent Probe for Lead Ion Assays. Macromol Rapid Commun 28(12):1333–1338
33. Varazo K, Xie F, Gulledge D, Wang Q (Sep. 2008) Synthesis of triazolyl anthracene as a selective fluorescent chemosensor for the Cu(II) ion. Tetrahedron Lett 49(36):5293–5296
34. Lin Y-I, Lang SA, Seifert CM, Child RG, Morton GO, Fabio PF Aldehyde Syntheses. Study of the preparation of 9,10-anthracenedicarboxaldehyde. J Organomet Chem 44(25):4701–4703 décembre 1979
35. Ryan DK, Weber JH (May 1982) Fluorescence quenching titration for determination of complexing capacities and stability constants of fulvic acid. Anal Chem 54(6):986–990